Journal of Power Sources 252 (2014) 79–84

Contents lists available at ScienceDirect

Journal of Power Sources

journal homepage: www.elsevier.com/locate/jpowsour

High-efficiency intermediate temperature solid oxide electrolyzer cells for the conversion of carbon dioxide to fuels

Jingbo Yan [a,b], Hao Chen [c], Emir Dogdibegovic [c], Jeffry W. Stevenson [d], Mojie Cheng [a,*], Xiao-Dong Zhou [c,*]

[a] Division of Fuel Cells, Dalian National Laboratory for Clean Energy, Dalian Institute of Chemical Physics, Chinese Academy of Sciences, Dalian 116023, China
[b] University of Chinese Academy of Sciences, Beijing 100049, China
[c] Department of Chemical Engineering, University of South Carolina, Columbia, SC 29028, USA
[d] Pacific Northwest National Laboratory, Richland, WA 99352, USA

HIGHLIGHTS

- Cell area specific resistance was current-dependent during high temperature CO_2 reduction.
- Ni–YSZ electrode showed higher resistance in SOEC mode than SOFC mode.
- The temperature drop at thermal minimum voltage created the condition for coking on Ni–YSZ.
- Higher temperature and higher CO_2 partial pressure could help minimize coking on Ni–YSZ.

ARTICLE INFO

Article history:
Received 9 August 2013
Received in revised form
23 October 2013
Accepted 20 November 2013
Available online 1 December 2013

Keywords:
High temperature electrolysis
CO_2 reduction
Distribution of relaxation times analysis
Carbon deposition

ABSTRACT

Electrochemical reduction of carbon dioxide in the intermediate temperature region was investigated by utilizing a reversible solid oxide electrolysis cell (SOEC). The current–potential (i–V) curve exhibited a nonlinear characteristic at low current density. Differentiation of i–V curves revealed that the cell area specific resistance (ASR) was current-dependent and had its maximum in electrolysis mode and minimum in fuel cell mode. Impedance measurements were performed under different current densities and gas compositions, and the results were analyzed by calculating the distribution of relaxation times. The ASR variation resulted from the difference in electrochemical reactions occurring on the Ni–YSZ electrode, *i.e.*, Ni–YSZ is a better electrode for CO oxidation than for CO_2 reduction. Coke formation on Ni–YSZ played a crucial role in affecting its electrolysis performance in the intermediate temperature region. The ASR apex was associated with a decrease in cell temperature during electrolysis due to the endothermic nature of CO_2 reduction reaction. It was postulated that such a decrease in temperature and rise in CO concentration led to coke formation. As a consequence, higher temperature (>700 °C), higher CO_2 concentration (>50%), and the presence of hydrogen or steam are recommended for efficient CO_2 reduction in solid oxide electrochemical cells.

1. Introduction

The conversion of renewable electrical energy to fuels using common substrates (e.g. CO_2 and water) provides an opportunity to remove the temporal variation in the energy supply from solar and wind energy sources. As a consequence, electrolysis has gained substantial attention to convert water and/or carbon dioxide to fuels. In comparison with room temperature electrolysis techniques, the essence of solid oxide electrolyzer cells (SOECs) lies at its elevated operation temperatures (>650 °C), which result in (1) a higher electrolysis efficiency because of a lower Nernst potential – a thermodynamic potential required to split CO_2 – at higher operation temperatures, and (2) the use of inexpensive oxide-based electrodes as the catalysts for a cost-effective electrolysis, instead of the precious metals (e.g. Pt) used in solution-based electrolysis cells [1]. An additional advantage of conversion of CO_2 to CO in SOECs is their capability of generating oxygen where water is not available, for instance during the exploration of the Planet Mars [2,3]. Furthermore, the high temperature CO_2 electrolysis can be

* Corresponding authors.
E-mail addresses: mjcheng@dicp.ac.cn (M. Cheng), xiao-dong.zhou@sc.edu (X.-D. Zhou).

0378-7753/$ – see front matter © 2013 Elsevier B.V. All rights reserved.
http://dx.doi.org/10.1016/j.jpowsour.2013.11.047

integrated with carbon fixation and syngas production, whereas syngas can undergo Fischer–Tropsch process to yield hydrocarbon fuels, thus facilitating a carbon-neutral cycle [4–8].

The primary challenge in developing SOECs is their degradation at elevated temperatures when LSM/YSZ was used as the air electrode, largely due to the delamination of air electrode [9–11] and the formation of pores at YSZ grain boundary [12]. $La_{1-x}Sr_xCo_{1-y}Fe_yO_{3-\delta}$ (LSCF), on the other hand, was found to be capable of suppressing the delamination problem [13]. Tietz et al. [14] recently reported a degradation rate of 3.8% per 1000 h over 9000 h at 778 °C for steam electrolysis with LSCF as the oxygen electrode. Since most works on high temperature electrolysis were carried out at approximately 800 °C or higher, the aim of the present research was to study the electrochemical reduction of CO_2 over the intermediate temperature regime (650–750 °C). LSCF was used as the air electrode, which can provide sufficient activity and less degradation in this temperature region. The results were analyzed by the differentiation of *i*–*V* curve [15] for DC measurements and the distribution of relaxation times (DRT) [16–20] for impedance measurements.

2. Experimental

A bilayer comprised of Ni–YSZ and YSZ electrolyte was prepared by tape casting. The thickness and diameter of the bilayers were approximately 1 mm and 25 mm, respectively, and the dense electrolyte membrane was ~8 μm thick. A $Gd_{0.20}Ce_{0.80}O_{1.90}$ (GDC, Fuel cell materials, OH) layer was spin-coated on YSZ and co-sintered with anode current collector (Ni mesh embedded in NiO paste) at 1150 °C for 2 h. Micrometer carbon powders were added as a pore former for $(La_{0.60}Sr_{0.40})_{0.995}(Co_{0.20}Fe_{0.80})O_{3-x}$ (LSCF, Fuel cell materials, OH) and $(La_{0.8}Sr_{0.2})_{0.95}MnO_{3-x}$ (LSM20, NexTech Materials, OH) inks. A layer of LSCF with 10 wt.% carbon was screen-printed on the GDC layer; then another layer of LSCF containing 20 wt.% carbon was added on the first layer. After sintering the LSCF at 900 °C for 2 h, LSM20 containing 50 wt.% carbon was screen-printed as the current collecting layer, and a piece of gold mesh was pressed into the wet LSM20 ink before heating up. The active cathode area was 2 cm^2 for calculating current density and area specific resistance (ASR). Fig. 1 shows a schematic illustration and a cross-sectional image of the cell structure.

Each cell was electrically connected to the test fixture with Pt wires, and then sealed on a tubular alumina stand with a glass paste. A perforated alumina cap was laid on top of the gold mesh and spring-loaded to provide sufficient mechanical contact to the LSCF electrode. The fuel to the Ni–YSZ electrode was 25% CO–75% CO_2 or 50% CO–50% CO_2 at a flow rate of 200 sccm, and the LSCF electrode was supplied with 400 sccm air. Solartron 1470E Multistat and 1255B Frequency Response Analyzer (Solartron Analytical, TN) were used for *i*–*V* sweep and impedance measurement. The AC amplitude was either 5 mV at OCV or 5% of the applied direct current (from 0 up to ±0.4 A cm^{-2}) for impedance measurements ranging from 0.01 to 100 kHz. Cells were tested at 650, 700 and 750 °C.

3. Results and discussion

The *i*–*V* curves and impedance spectra are illustrated in Figs. 2 and 3, respectively. Open circuit voltages were very close to the theoretical Nernst potentials, indicating the presence of a hermetic seal. All *i*–*V* curves evolve smoothly from SOFC to SOEC mode in a nonlinear manner within the sweep range. Hence, the cell ASR, defined as dE_i/di, varies with current density. Impedance spectra in Fig. 3 show that the polarization resistance (R_p) decreased monotonously in proportion to the current density when the cell was operated in fuel cell mode (e.g. under positive current). With the presence of negative current, *i.e.* electrolysis mode, R_p pattern was more complex. At 650 °C, R_p is found to decrease with increasing current density; while at 700 and 750 °C, R_p first increases at lower current density and then decreases at higher current density. It is also noticed that the ohmic resistance (R_Ω) increases in SOEC mode and decreases in SOFC mode with increasing current density. The deviated R_Ω could recover when the DC bias was removed, suggesting that it is a temporal effect under polarization. Such minor change of R_Ω with DC bias was observed in other studies [21,22], and its reason will be discussed further. Since the R_Ω variation was minor compared to R_p, the change of R_p dominated the change of ASR of the cell. The differentiation of the *i*–*V* curve yields the total ASR of the cell. In our previous study [15] the ASR values derived from the differentiation of *i*–*V* curve were compared to results from impedance measurements, and showed good agreement, thus analysis of impedance spectra can provide more details on the electrochemical processes occurring in SOECs.

Fig. 4 shows the total ASR of the cell measured by *i*–*V* sweep. The $ASR_{t,dc}$ exhibited a maximum in SOEC mode and a minimum in SOFC mode. Moreover, the fuel rich in CO resulted in larger resistance. Such a phenomenon became more prominent at lower temperatures due to its thermally activated conversion process, which will be discussed further. Ebbesen and Mogensen [23] also observed the similar phenomenon on a LSM–YSZ based cell, with an ASR of 0.30 Ω cm^2 and 0.36 Ω cm^2 for SOFC and SOEC, respectively (850 °C, CO_2/CO = 50/50, ±0.25 A cm^{-2}). The change in gas composition influenced the ASR of SOEC more than that of SOFC. For instance, the difference in ASR between the fuels consisting of 25% CO and 50% CO was negligible at 700 °C when the current density increased from 0 to 0.4 A cm^{-2}; however in SOEC mode, the ASR between the two fuels differed as much as 0.2 Ω cm^2. Such an ASR change in SOEC mode was even more pronounced at 650 °C. In all experiments, switching fuel gas from 25% CO–75% CO_2 to 50% CO–50% CO_2 resulted in a higher ASR, suggesting that certain electrochemical processes on Ni–YSZ are responsible for the increase of ASR in SOEC mode. The analysis of DC measurement alone, however, cannot provide sufficient information on the origin of this phenomenon. The deconvolution of impedance spectra by analyzing the distribution of relaxation times (DRT) [17] becomes necessary, because this approach is capable of resolving overlapping arcs up to half a decade.

Fig. 5 illustrates DRT spectra derived from the imaginary part of the impedance data measured at 700 °C. The area under the curve represents the total polarization resistance, and each peak represents a process that contributes to the R_p. In the current case (700 °C and CO 50%–CO_2 50%), five peaks at 4073 Hz, 581 Hz, 38.9 Hz, 2.4 Hz and 0.1 Hz were observed and designated as P1 to P5, respectively. Such relaxation times distribution pattern is typical for a solid oxide cell with Ni–YSZ and LSCF electrodes. Leonide and Ivers-Tiffee [24] attributed the peaks at 2.3 kHz, 581 Hz, and 4.1 Hz to ionic transport, charge transfer, and gas diffusion in the anode, respectively. The peak at 16.2 Hz represents oxygen surface exchange and bulk diffusion in the cathode. Cathode gas diffusion is represented by the peak at 0.1 Hz. The aforementioned peak attribution serves as a framework for our analysis. P1, P2 and P3 shown in Fig. 5 dominate the spectrum measured under OCV. When the cell was operated with a positive current (SOFC mode), P2 and P3 were reduced by about 60%. A negative current (SOEC mode), however, resulted in a significant decrease in P3 while an increase in P2. The response of P2 to various operation modes appears interesting as it corresponds to electrochemical catalytic characteristics of the cell, *i.e.* whether it favors CO oxidation or CO_2 reduction. In order to identify the origin of this peak,

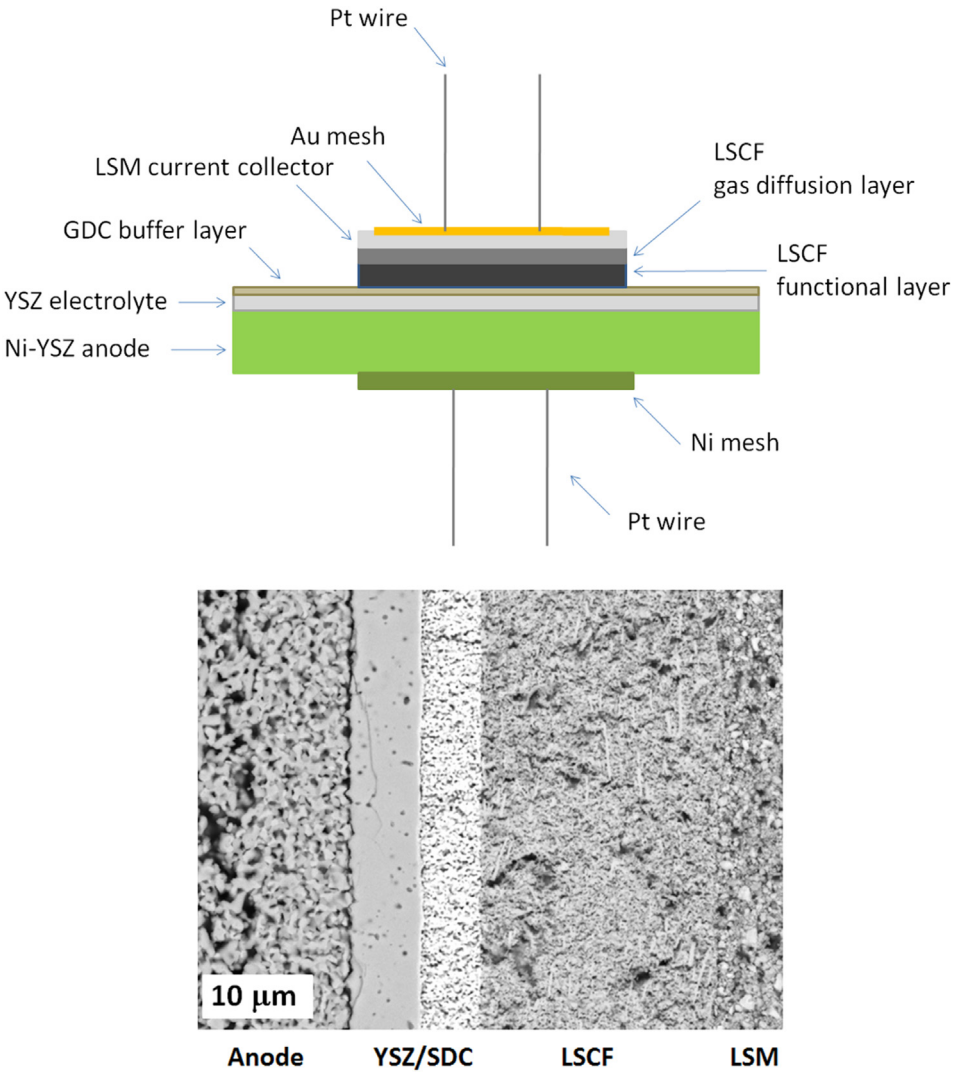

Fig. 1. A schematic illustration and a cross sectional image of the cell structure.

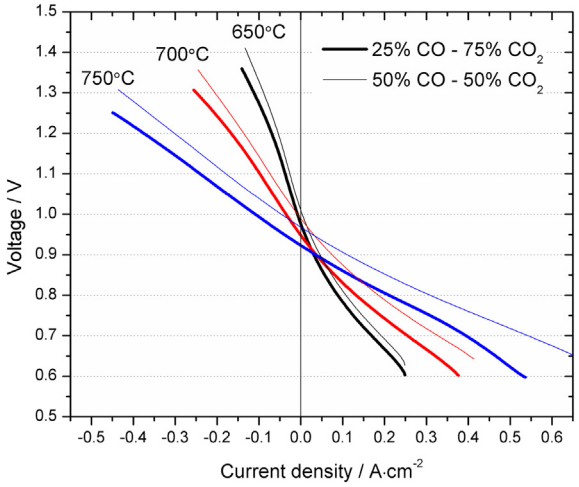

Fig. 2. *V–i* curves for Ni–YSZ/YSZ/GDC/LSCF cell at different temperatures and feed compositions: (thick lines) 25% CO–75% CO_2; (thin lines) 50% CO–50% CO_2.

data measured under different gas compositions and DC bias are analyzed and compared.

DRT transformation of impedance data measured under negative current was performed to examine the contributions of polarization resistance. The result in Fig. 6 showed that as gas composition shifted from 25% CO–75% CO_2 to 50% CO–50% CO_2, P2 at 316 Hz increased and P1 at 4 kHz decreased. This was observed at both 650 °C and 700 °C. Since the change of gas composition occurred in the fuel side while the air side remained the same, hence the increase in ASR was a result of the electrochemical processes on Ni–YSZ electrode. Consequently, it is reasonable to attribute P1 and P2 to the Ni–YSZ electrode. Similar assignment was carried out by Leonide et al. on an anode-supported SOFC [24], in which the impedance arc at 581 Hz was ascribed as gas diffusion coupled with charge transfer and ionic transport in anode functional layer.

Wang and Gorte [25] compared LSM, LSF and LSCo as the oxygen electrode for solid oxide electrolyzer and observed that ASR was independent of current density up to 140 mA cm^{-2}. Since the LSCF used in this work possesses similar properties with LSC or LSF, it is reasonable to assume that the oxygen electrode is not responsible for the current dependency observed in our study, at least in the range of ±0.1 mA cm^{-2}. On the other hand, Kim-Lohsoontorn et al. [26] studied a Ni–GDC based cell, which exhibited a better

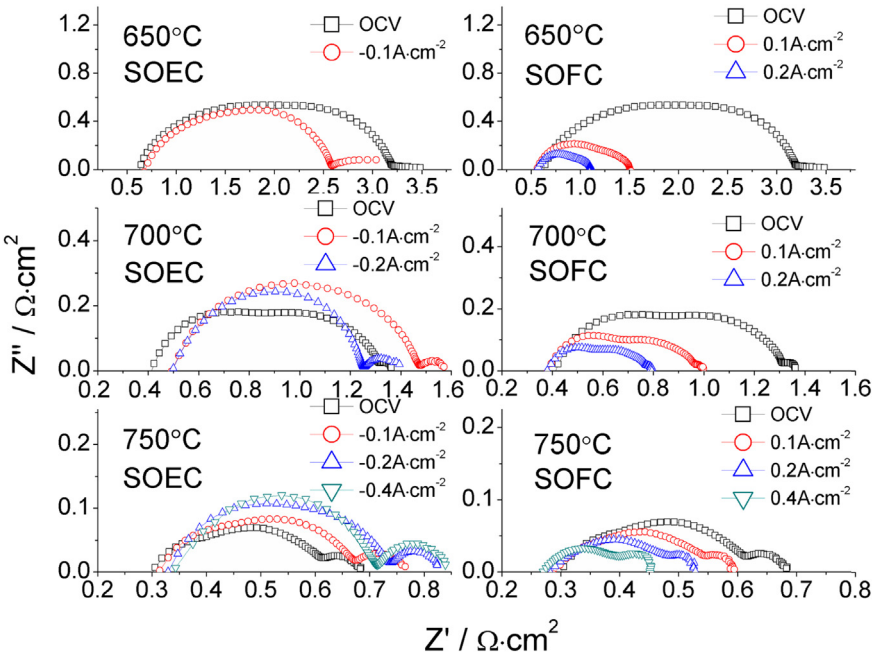

Fig. 3. Impedance measured for Ni–YSZ/YSZ/GDC/LSCF cell under 50% CO–50% CO_2: (left) SOEC mode; (right) SOFC mode.

performance as an electrolyzer than a fuel cell. They attributed this observation to the oxygen storage capacity of GDC, which likely suppressed the oxidation of Ni surface. Replacing Ni–YSZ with Ni–GDC resulted in different current-dependency pattern of cell resistance suggests that such a current-dependent feature most likely originated from the fuel electrode.

It is known that direct CO_2 electrolysis on Ni–YSZ is kinetically sluggish compared to other reactions such as water splitting [27,28], implying that the direct electrochemical reduction of CO_2 on Ni–YSZ is intrinsically a rate-limiting process. Moreover, Stoots et al. [5] suggested that coke formation is possible, since the CO_2 reduction potential is only slightly lower than that of coke formation reaction:

$$CO \rightarrow C + 0.5O_2 \quad [1]$$

Under SOEC operating conditions, the latter becomes even more feasible. If such a thermodynamic condition was reached, it can lead to coke deposition on the catalytically active sites because nickel is capable of catalyzing CO disproportionation reaction, also known as Boudouard reaction:

$$2CO \rightarrow C + CO_2 \quad [2]$$

This may explain why the 25% CO–75% CO_2 composition, which had a lower CO partial pressure, resulted in a lower SOEC ASR. However, the fact that ASR decreased after reaching the peak value implies that CO partial pressure is not the only factor. Interestingly, by plotting the ASR against voltage (Fig. 7), it is noticed that all maximum ASR values were reached at a similar voltage for three different temperatures, *i.e.* 1.08 V for 25% CO–75% CO_2 and 1.11 V for

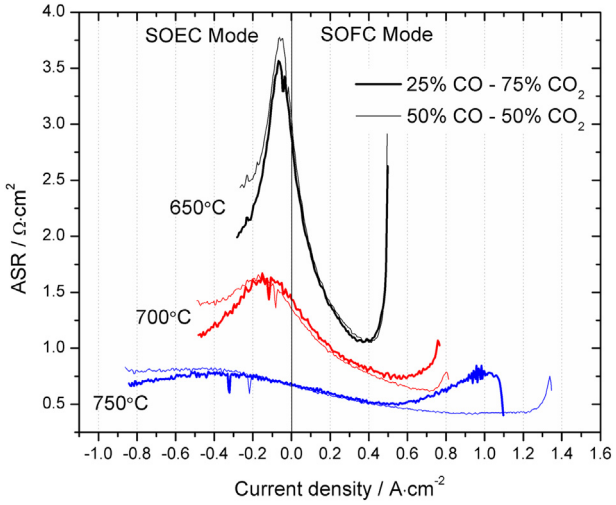

Fig. 4. ASR vs. current density plots, derived from differentiation of *V–i* curves measure for Ni–YSZ/YSZ/GDC/LSCF cell: (thick lines) 25% CO–75% CO_2; (Thin lines) 50% CO–50% CO_2.

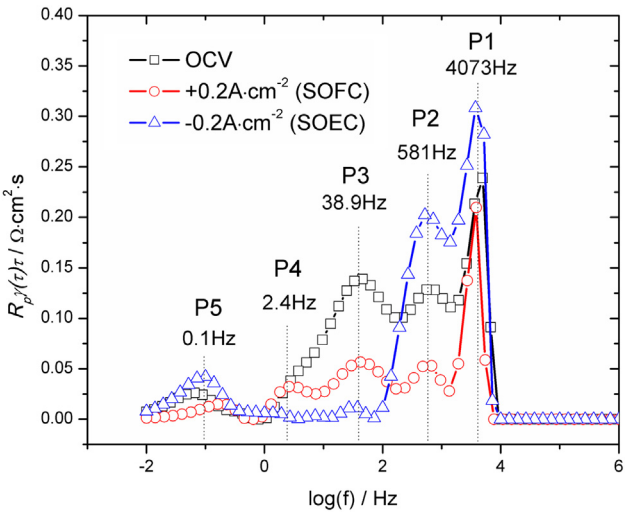

Fig. 5. DRT spectra for Ni–YSZ/YSZ/GDC/LSCF cell measured under 700 °C and 50% CO–50% CO_2: (-□-) OCV; (-○-) +0.2 A cm^{-2}; (-△-) −0.2 A cm^{-2}.

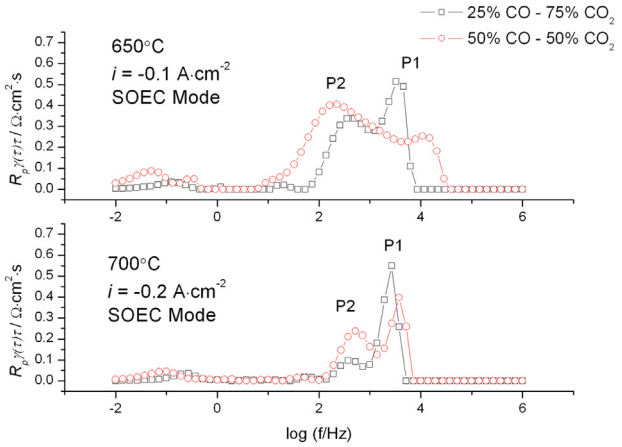

Fig. 6. DRT spectra showing the effect of shifting gas composition under electrolytic current at 650 °C and 700 °C for Ni–YSZ/YSZ/GDC/LSCF cell: (-□-) 25% CO–75% CO_2; (-○-) 50% CO–50% CO_2.

50% CO–50% CO_2. Since electrolysis is an endothermic process, the heat required for the reaction increases linearly with current density while the heat generated from Joule effect is proportional to the square of current density. Thus, the heat demand of the reaction can be compensated by Joule heat at a certain voltage, referred to as thermal neutral voltage (TNV), which is slightly dependent of temperature but independent of gas composition. The TNVs for CO_2 electrolysis at 650, 700 and 750 °C are 1.466, 1.465 and 1.464 V, respectively. Therefore, as the cell voltage increases, a minimum temperature is expected somewhere between OCV and TNV.

In an SOEC model [29] developed for CO_2 electrolysis, the mean electrolyte temperature was found to initially decrease with voltage, reaching the minimum at about 1.1 V, and then increase significantly afterwards, eventually leveling up with the inlet gas temperature at TNV. This temperature–voltage pattern is quite similar to the ASR-voltage pattern observed in our study. The minimum temperature is reached at 1.1 V, which agrees with results obtained in this research, where the ASR maximum value was at 1.08–1.11 V. This implies that the ASR maximum may be a result of temperature variation within the cell. In the simulation, the mean electrolyte temperature decreased by approximately 8 °C. A greater temperature decrease, however, could be expected at the electrode surface, particularly at the catalytically active sites, where the endothermic reaction takes place. O'Brien and co-workers [30] measured the temperature in a steam electrolyzer stack with a miniature thermocouple placed in the gas flow channel. They observed that the temperature decreased by ~11 °C at the thermal minimum voltage of 1.06 V, a voltage consistent with our observation. Since the enthalpy change (ΔH) of the electrochemical reaction is composed of two parts:

$$\Delta H = \Delta G + T\Delta S \quad [3]$$

where ΔG represents the electrical energy and $T\Delta S$ represents the thermal energy, it must be pointed out that CO_2 electrolysis presents greater thermal demand ($T\Delta S$) than H_2O, e.g. at 700 °C, $T\Delta S$ are 84.79 kJ mol^{-1} and 53.35 kJ mol^{-1} for CO_2 and H_2O reduction, respectively. Hence for CO_2 electrolysis, it is reasonable to assume that the temperature at the electrode surface could be lowered by more than 11 °C at the thermal minimum voltage. Moreover, the temperature shift is further supported by the impedance results in Fig. 3, which show that R_Ω increases in SOEC mode as a result of cooling and decreases in SOFC mode as a result of heating at all temperatures and in all gas compositions.

The decrease in temperature would certainly lower the electrode activity to some extent, yet under the conditions given in this study, it may well trigger critical equilibrium shift that leads to carbon deposition, particularly at temperature ~650 °C. According to Boudouard's equilibrium (see Fig. 8), the equilibrate fraction of CO at 650 °C is 39%, therefore, any higher CO concentration would result in carbon formation. Obviously in our case, the 50% CO–50% CO_2 fuel gas composition already exceeded the limit, making the Ni–YSZ electrode prone to carbon deposition.

When the electrolytic current was applied, the CO/CO_2 ratio on the electrode surface further increased. This effect together with the decrease in temperature rapidly brought down the equilibrate fraction of CO, and facilitate coke formation on the electrode. As a consequence, some catalytic active sites are blocked and subsequently the cell resistance is increased. With further increasing the electrolytic current, it was possible to offset the coking tendency of the system by recovering temperature and accelerating mass transfer. At 700 and 750 °C, the equilibrate CO fractions are 57% and 74%, respectively, higher than the 50% CO in the fuel gas.

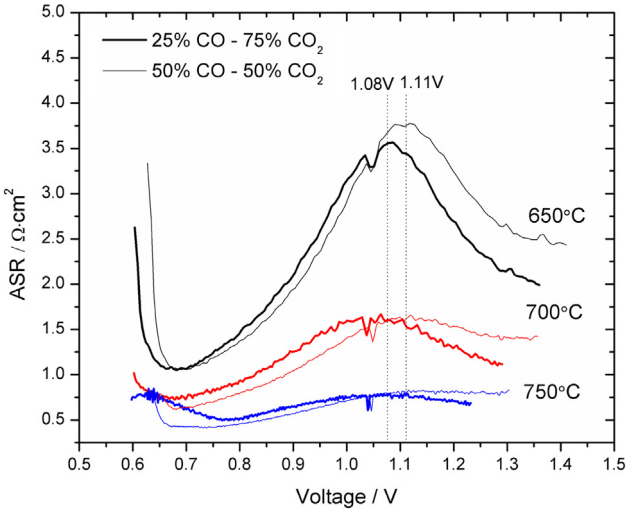

Fig. 7. ASR vs. voltage plots: (Thick lines) 25% CO–75%CO_2; (Thin lines) 50% CO–50% CO_2. The ASR peaks for 25% CO–75% CO_2 appeared at 1.08 V, and the peaks for 50% CO–50%CO_2 appeared at 1.11 V.

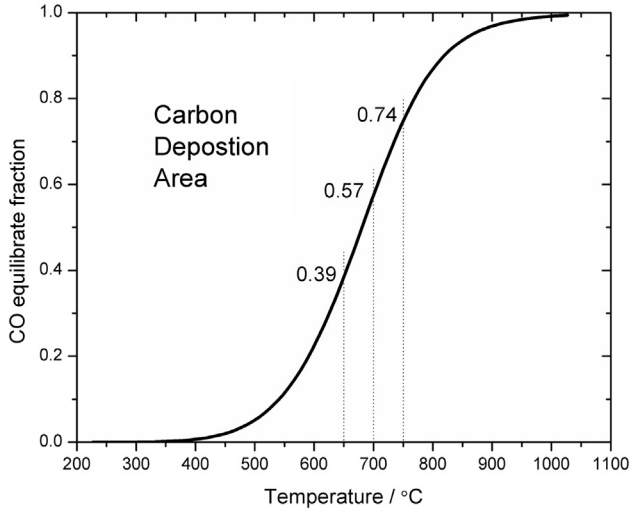

Fig. 8. Boudouard equilibrium. The area above the curve indicates carbon deposition zone; the CO equilibrate fractions for 650 °C, 700 °C, 750 °C are 0.39, 0.57, 0.74, respectively.

Consequently, the ASR peaks at 700 and 750 °C were much lower. The temperature drop was probably the major cause of the ASR increase in these cases, and coke formation was not triggered.

Hence, in order to improve the performance towards CO_2 reduction, it is necessary to operate the cell at higher temperatures (>700 °C) and higher CO_2 concentration (>50%) to avoid possible coking. Addition of water can suppress coke formation on the electrode. Indeed, co-electrolysis of steam and CO_2 exhibited similar performance as steam electrolysis [4,7,31–33], suggesting water splitting to form hydrogen is more preferred and CO is produced by the following reverse water–gas shift reaction. Therefore mixing CO_2 feed gas with steam or hydrogen is a feasible approach to improve the electrolysis efficiency.

4. Conclusions

The performance of Ni–YSZ/YSZ/GDC/LSCF cell for CO_2 electrolysis at intermediate temperature (650–750 °C) was investigated with *V–i* curve differentiation and distribution of relaxation times for DC and AC data, respectively. Results suggest that cell ASR was current-dependent, ascending to a maximum during electrolysis and descending to a minimum in SOFC operation. This phenomenon was associated with electrolysis induced temperature drop that not only caused lower cell activity but also possible coke formation on Ni–YSZ, particularly at 650 °C. Therefore, temperature above 700 °C and CO_2 concentration higher than 50% are recommended for CO_2 electrolysis at intermediate temperatures. Furthermore, the addition of H_2 and steam could also improve the efficiency of CO_2 reduction.

Acknowledgements

This work was supported by the Solid State and Materials Chemistry Program of the Division of Materials Research at the National Science Foundation under Grant Number DMR-1006113.

References

[1] A. Hauch, S.D. Ebbesen, S.H. Jensen, M. Mogensen, J. Mater. Chem. 18 (2008) 2331–2340.
[2] K.R. Sridhar, C.S. Iacomini, J.E. Finn, J. Propul. Power 20 (2004) 892–901.
[3] K.R. Sridhar, B.T. Vaniman, Solid State Ionics 93 (1997) 321–328.
[4] Z. Zhan, W. Kobsiriphat, J.R. Wilson, M. Pillai, I. Kim, S.A. Barnett, Energy Fuels 23 (2009) 3089–3096.
[5] C. Stoots, J. O'Brien, J. Hartvigsen, Int. J. Hydrogen Energy 34 (2009) 4208–4215.
[6] J.E. O'Brien, M.G. McKellar, E.A. Harvego, C.M. Stoots, Int. J. Hydrogen Energy 35 (2010) 4808–4819.
[7] C. Graves, S.D. Ebbesen, M. Mogensen, Solid State Ionics 192 (2011) 398–403.
[8] C. Graves, S.D. Ebbesen, M. Mogensen, K.S. Lackner, Renewable Sustainable Energy Rev. 15 (2011) 1–23.
[9] K.F. Chen, N. Ai, S.P. Jiang, J. Electrochem. Soc. 157 (2010) P89–P94.
[10] K.F. Chen, S.P. Jiang, Int. J. Hydrogen Energy 36 (2011) 10541–10549.
[11] M. Keane, M.K. Mahapatra, A. Verma, P. Singh, Int. J. Hydrogen Energy 37 (2012) 16776–16785.
[12] R. Knibbe, M.L. Traulsen, A. Hauch, S.D. Ebbesen, M. Mogensen, J. Electrochem. Soc. 157 (2010) B1209–B1217.
[13] G. Schiller, A. Ansar, M. Lang, O. Patz, J. Appl. Electrochem. 39 (2009) 293–301.
[14] F. Tietz, D. Sebold, A. Brisse, J. Schefold, J. Power Sources 223 (2013) 129–135.
[15] X.D. Zhou, L.R. Pederson, J.W. Templeton, J.W. Stevenson, J. Electrochem. Soc. 157 (2010) B220–B227.
[16] H. Schichlein, A.C. Muller, M. Voigts, A. Krugel, E. Ivers-Tiffee, J. Appl. Electrochem. 32 (2002) 875–882.
[17] B. Liu, H. Muroyama, T. Matsui, K. Tomida, T. Kabata, K. Eguchi, J. Electrochem. Soc. 157 (2010) B1858–B1864.
[18] B. Liu, H. Muroyama, T. Matsui, K. Tomida, T. Kabata, K. Eguchi, J. Electrochem. Soc. 158 (2011) B215–B224.
[19] V. Sonn, A. Leonide, E. Ivers-Tiffee, J. Electrochem. Soc. 155 (2008) B675–B679.
[20] A. Leonide, V. Sonn, A. Weber, E. Ivers-Tiffee, J. Electrochem. Soc. 155 (2008) B36–B41.
[21] X.J. Chen, K.A. Khor, S.H. Chan, Solid State Ionics 167 (2004) 379–387.
[22] P. Kim-Lohsoontorn, D.J.L. Brett, N. Laosiripojana, Y.M. Kim, J.M. Bae, Int. J. Hydrogen Energy 35 (2010) 3958–3966.
[23] S.D. Ebbesen, M. Mogensen, J. Power Sources 193 (2009) 349–358.
[24] A. Leonide, B. Ruger, A. Weber, W.A. Meulenberg, E. Ivers-Tiffee, J. Electrochem. Soc. 157 (2010) B234–B239.
[25] W.S. Wang, Y.Y. Huang, S.W. Jung, J.M. Vohs, R.J. Gorte, J. Electrochem. Soc. 153 (2006) A2066–A2070.
[26] P. Kim-Lohsoontorn, N. Laosiripojana, J. Bae, Curr. Appl. Phys. 11 (2011) S223–S228.
[27] Y. Jiang, A.V. Virkar, J. Electrochem. Soc. 150 (2003) A942–A951.
[28] C.M. Stoots, J.E. O'Brien, K.G. Condie, J.J. Hartvigsen, Int. J. Hydrogen Energy 35 (2010) 4861–4870.
[29] M. Ni, Chem. Eng. J. 164 (2010) 246–254.
[30] J.E. O'Brien, J. Heat Transfer 134 (2012) 031017, 031017.
[31] S.D. Ebbesen, C. Graves, M. Mogensen, Int. J. Green Energy 6 (2009) 646–660.
[32] P. Kim-Lohsoontorn, J. Bae, J. Power Sources 196 (2011) 7161–7168.
[33] C.M. Stoots, J.J. Hartvigsen, J.E. O'Brien, J.S. Herring, J. Fuel Cell Sci. Technol. 6 (2008) 011014, 011014.